JOURNAL OF VIROLOGY, Nov. 2010, p. 11395–11406 Vol. 84, No. 21
0022-538X/10/$12.00 doi:10.1128/JVI.01047-10

An RNA Pseudoknot Is Required for Production of Yellow Fever Virus Subgenomic RNA by the Host Nuclease XRN1[▽]

Patrícia A. G. C. Silva, Carina F. Pereira,† Tim J. Dalebout, Willy J. M. Spaan, and Peter J. Bredenbeek*

Department of Medical Microbiology, Center of Infectious Diseases, Leiden University Medical Center, P.O. Box 9600, 2300 RC Leiden, Netherlands

Received 14 May 2010/Accepted 9 August 2010

Cells and mice infected with arthropod-borne flaviviruses produce a small subgenomic RNA that is colinear with the distal part of the viral 3′-untranslated region (UTR). This small subgenomic flavivirus RNA (sfRNA) results from the incomplete degradation of the viral genome by the host 5′-3′ exonuclease XRN1. Production of the sfRNA is important for the pathogenicity of the virus. This study not only presents a detailed description of the yellow fever virus (YFV) sfRNA but, more importantly, describes for the first time the molecular characteristics of the stalling site for XRN1 in the flavivirus genome. Similar to the case for West Nile virus, the YFV sfRNA was produced by XRN1. However, in contrast to the case for other arthropod-borne flaviviruses, not one but two sfRNAs were detected in YFV-infected mammalian cells. The smaller of these two sfRNAs was not observed in infected mosquito cells. The larger sfRNA could also be produced *in vitro* by incubation with purified XRN1. These two YFV sfRNAs formed a 5′-nested set. The 5′ ends of the YFV sfRNAs were found to be just upstream of the previously predicted RNA pseudoknot PSK3. RNA structure probing and mutagenesis studies provided strong evidence that this pseudoknot structure was formed and served as the molecular signal to stall XRN1. The sequence involved in PSK3 formation was cloned into the Sinrep5 expression vector and shown to direct the production of an sfRNA-like RNA. These results underscore the importance of the RNA pseudoknot in stalling XRN1 and also demonstrate that it is the sole viral requirement for sfRNA production.

The *Flavivirus* genus contains nearly 80 viruses distributed worldwide and includes important human pathogens such as dengue virus (DENV), yellow fever virus (YFV), Japanese encephalitis virus (JEV), West Nile virus (WNV), and tick-borne encephalitis virus (TBEV). Phylogenetic analysis clustered flaviviruses into the following three major groups, based on the vector of transmission: (i) mosquito-borne viruses, (ii) tick-borne viruses, and (iii) viruses with no known vector (NKV) (13, 26).

Flaviviruses are small enveloped viruses containing a positive-sense single-stranded RNA genome of approximately 11 kb in length, with a 5′ cap structure and a 3′ nonpolyadenylated terminus. The genomic RNA is flanked by 5′- and 3′-untranslated regions (UTRs) and encodes a single polyprotein that is co- and posttranslationally processed by viral and cellular proteases into three structural proteins (C, prM, and E) and seven nonstructural proteins (NSs) (reviewed in reference 30). Apart from the viral genomic RNA and the replication-related replicative-form and intermediate RNAs (11, 12), an additional small flavivirus RNA (sfRNA) has been detected in mice and both mammalian and insect cells infected with flaviviruses belonging to the JEV serogroup (29, 49, 56). Recently, it was shown that production of sfRNA is not unique to JEV and closely related viruses but that all arthropod-borne flaviviruses generate an sfRNA upon infection of mammalian cells (31, 44). The lengths of these sfRNAs vary from 0.3 kb to 0.5 kb and are related to the length of the viral 3′ UTR. Surprisingly, these sfRNAs are not direct products of the viral transcription mechanism but result from incomplete degradation of the viral genomic RNA by the host 5′-3′ exonuclease XRN1, as shown for Kunjin virus (KUNV) by *in vitro* assays and RNA interference (RNAi) experiments. Although the exact role of the sfRNA in the viral life cycle is still elusive, production of sfRNA was shown to be essential for KUNV cytopathogenicity in cell culture and for viral pathogenicity in infected mice (44).

XRN1 is well conserved among eukaryotes and is the main cytoplasmic RNase associated with 5′-3′ mRNA decay that takes place in cytoplasmic processing bodies (P bodies), where the mRNA is decapped by the enzymes DCP1 and -2 and subsequently degraded 5′ to 3′ by XRN1 (reviewed in references 2, 19, 21, and 50). XRN1 acts in a processive manner by hydrolyzing RNA with 5′-monophosphate end groups to 5′-mononucleotides (53, 54). Based on fluorescence *in situ* hybridization (FISH) analysis of KUNV-infected cells, the sfRNA was reported to colocalize with XRN1 in P bodies (44). Interestingly, the role of XRN1 in a viral life cycle is not limited to flaviviruses. XRN1 has also been shown to have an antiviral activity by virtue of its exonuclease activity (18) and to act as a potent suppressor of viral RNA recombination in viruses such as tomato bushy stunt virus (10). Studies have shown that XRN1 can be blocked to some degree by elements such as a poly(G) tract sequence or large, stable RNA stem-loop structures (15, 38, 58). The 3′ UTR of the mosquito-borne flaviviruses is predicted to fold into a highly complex structure involving well-conserved RNA sequences as

* Corresponding author. Mailing address: Department of Medical Microbiology, Leiden University Medical Center, P.O. Box 9600, 2300 RC Leiden, Netherlands. Phone: 317 1526 1652. Fax: 317 1526 6761. E-mail: P.J.Bredenbeek@lumc.nl.

† Present address: Department of Pathology, University of Cambridge, Tennis Court Road, Cambridge CB2 1QP, United Kingdom.

▽ Published ahead of print on 25 August 2010.

well as strong secondary structures, such as the long 3′ stem-loop (3′ SL) and one or two dumbbell-like RNA structures (22, 41; for a review, see reference 32). In addition, several RNA pseudoknots are predicted within the mosquito-borne flavivirus 3′ UTR (41, 51). Sequence alignments and computer-aided folding of several flavivirus 3′ UTRs indicated that the production of sfRNA most likely results from the stalling of XRN1 at a conserved RNA stem-loop structure designated SL-II. Deletions in the KUNV 3′ UTR that include SL-II abolished the production of KUNV sfRNA (44).

To determine the involvement of the flavivirus 3′ UTR SL-II structure in sfRNA generation, we performed a detailed analysis of sfRNA production in YFV-infected cells and mapped the XRN1 stalling site by using site-directed mutagenesis of a YFV-17D infectious clone and RNA structure probing. From our data, we concluded that YFV infection of mammalian cells results in the XRN1-mediated production of two sfRNAs that form a 5′-nested set. More importantly, we demonstrated that an RNA pseudoknot involving the YFV equivalent of SL-II is required for stalling of XRN1 and therefore crucial for the generation of the flavivirus sfRNAs.

MATERIALS AND METHODS

Cell culture. The origin and culture conditions of the BHK-21J, Vero E6, and SW13 cells used in this study have been described before (7, 52). C6/36 cells (23) were obtained from the ATCC and grown in Eagle's minimal essential medium (EMEM) supplemented with 8% fetal calf serum (Bodinco, Netherlands) and 5% nonessential amino acids.

Recombinant DNA techniques and plasmid construction. Unless explained in more detail, standard nucleic acid methodologies were used (3, 48). Chemically competent *Escherichia coli* DH5α cells (24) were used for cloning. YFV-17D nucleotide numbering was according to Rice et al. (47) (GenBank accession no. X03700).

Plasmid pBlsrcptSK-YFV$_{9845–10861}$ (R. Molenkamp et al., unpublished data), which contains the complete 3′ UTR of YFV-17D, was used as a template for site-directed mutagenesis using the QuikChange strategy (Stratagene) to introduce mutations into the sequences of stem-loop E (SL-E) or in the nucleotides predicted to be involved in the formation of RNA pseudoknot 3 (PSK3) (41). After sequencing to verify the presence of the introduced mutations and to exclude unintended nucleotide changes, the mutant pBlsrcptSK-YFV$_{9845–10861}$ derivatives were digested with SfiI and XbaI, and the 492-bp DNA fragments containing the mutated SL-E or PSK3 sequences were cloned into pACNR-FLYF17Da (37).

A 194-bp HindIII-XbaI fragment encompassing the region between nucleotides (nt) 10,520 and 10,714 in the 3′ UTR of YFV was isolated from pHYF5′3′IVΔRS (7) and cloned into pBluescript SK(−). The resulting plasmid, pBlsrcptSK-YFV$_{10520–10714}$, was used as a template to generate a minus-strand YFV RNA fragment for use as a probe in RNase protection assays.

Plasmid pSinrep5-YFV$_{10531–10611}$ was constructed by inserting a linker encompassing nt 10,531 to 10,611 of YFV flanked by an MluI and SphI adapter into MluI- and SphI-digested pSinrep5eGFP. The pSINrep5-YFV$_{10521–10662}$ recombinant was constructed by PCR. Plasmid pBlsrcptSK-YFV$_{9845–10861}$ was used as a template with oligonucleotides that contained either an MluI site (forward primer) or an SphI site (reverse primer). The resulting PCR product was cloned into MluI- and SphI-digested pSinrep5-eGFP (6).

Plasmid DNAs of the pACNR-FLYF17Da mutants and recombinant pSinrep5 were linearized with AflII and XhoI, respectively, and used for *in vitro* RNA transcription (52).

XRN1 RNA silencing. Stocks of lentivirus particles, each expressing a short hairpin RNA (shRNA) (TRCN-049675, TRCN-049676, or TRCN-049677) against the human XRN1 gene (GenBank accession no. NM_019001.3), and a lentivirus expressing the scrambled shRNA SHC-002 were prepared from the MISSIONTRC-Hs1.0 library (Sigma) according to the manufacturer's recommendations. The particle titers of the lentivirus stocks were determined using a p24 enzyme-linked immunosorbent assay (ELISA) (Zeptometrix).

To analyze the effect of XRN1 silencing on YFV sfRNA production, 5×10^5 SW13 cells were transduced with a combination of two different lentiviruses expressing one of the shRNAs specified above at a multiplicity of infection (MOI) of 5 (each) or with the SHC-002-expressing virus at an MOI of 10. At 72 h posttransduction, the cells were infected with YFV-17D at an MOI of 5, and 30 h later, the cells were lysed (16) and analyzed for the expression of the host XRN1 protein and actin by Western blotting (28) after PAGE on 5 and 10% gels, respectively. Antibodies directed against human XRN1 (Bethyl Laboratories) and actin (Santa Cruz) were used at dilutions of 1:5,000 and 1:2,000, respectively. Viral sfRNA production was analyzed by Northern blotting as described below.

***In vitro* XRN1 assay.** Plasmid pYF-R.luc2A-RP (25) was linearized with XhoI and used as a template for *in vitro* transcription of YFV replicon RNA in the absence of a cap analogue. To remove the 5′-triphosphate, 7 μg of transcript was incubated with tobacco acid pyrophosphatase (TAP; Epicentre) as specified by the manufacturer. The TAP-treated RNA was purified by phenol-chloroform extraction and ethanol precipitation. The pellet was dissolved in 16 μl H_2O and used for digestion with XRN1 (Terminator 5′-phosphate-dependent exonuclease; Epicentre) under the conditions described by the manufacturer. The units of XRN1 are indicated in the relevant figure.

RNA transfection and analysis of viral RNA synthesis. BHK-21J cells were transfected with 5 μg of full-length YFV-17D or Sinrep5 transcript as described previously (52). In general, 2.5 ml (approximately 1.5×10^6 cells) of the transfected BHK-21J cell suspension was seeded in a 35-mm plate. Total RNA was isolated from the transfected cells at 8 h postelectroporation (p.e.) for the recombinant Sinrep5-transfected cells and at 24 h p.e. for the YFV-transfected cells. Analysis of RNA synthesis by [^{3}H]uridine labeling was performed as described previously (7). Trizol (Invitrogen) was used for cell lysis and subsequent RNA purification. [^{3}H]uridine-labeled RNAs were denatured with glyoxal and analyzed in 0.8% agarose gels (48).

For Northern blotting, samples containing 10 μg of total RNA from electroporated cells or *in vitro*-transcribed XRN1-treated RNA mixed with 5 μg total RNA from BHK cells were denatured using formaldehyde, separated in a formaldehyde-containing 1.5% agarose gel, and blotted onto a Hybond-N$^+$ membrane (GE Healthcare) (48). The blots were hybridized with ^{32}P-labeled oligonucleotides as described previously (34, 57), except for the analysis of sfRNA production in the XRN1 silencing experiments, in which case randomly primed, [α-^{32}P]dATP-labeled cDNA fragments directed against the YFV 3′ UTR (nt 10,555 to 10,862) and the human glyceraldehyde-3-phosphate dehydrogenase (GAPDH) gene (GenBank accession no. NM_00246; nt 321 to 724) were used as probes in 5× SSC (1× SSC is 0.15 M NaCl plus 0.015 M sodium citrate) and 50% formamide at 42°C (34).

Virus stocks, infections, and plaque assays. Medium was harvested from transfected cells to obtain virus stocks when a complete cytopathic effect (CPE) was observed. YFV-17D infections and plaque assays were performed essentially as described before (52), except for the agarose in the overlay, which was replaced by 1.2% Avicel (33).

Primer extension assay. Primer extension analysis was performed as described by Sambrook et al. (48), with minor modifications. Total RNA (5 to 7 μg) from YFV or recombinant Sinrep5 RNA-transfected cells or XRN1-treated pYF-R.luc2A-RP transcript was annealed to ^{32}P-labeled oligonucleotide 1632 or 1648. Oligonucleotide 1632 is complementary to YFV nt 10,690 to 10,708, and oligonucleotide 1648 is complementary to YFV nt 10,580 to 10,598. After hybridization and subsequent ethanol precipitations, primer extension reactions were performed using 200 U of RevertAid H Minus Moloney murine leukemia virus reverse transcriptase (Fermentas) as described by the manufacturer. After 1 h of incubation at 42°C, the samples were treated with RNase A (10 μg/μl; Qiagen) and purified by phenol-chloroform extraction and ethanol precipitation. The primer extension products were analyzed in a denaturing 5% polyacrylamide–8 M urea sequencing gel. A ^{33}P-labeled Cycle Reader (Fermentas) sequence reaction mix using oligonucleotide 1632- or 1648-primed pBlsrcptSK-YFV$_{9845–10861}$ as a template was run in the same gel as the primer extension products and served as a size and sequence marker.

RNase protection assay. pBlscrptSK-YFV$_{10520–10714}$ was linearized using HindIII, purified by phenol-chloroform extraction, and used as a template for T7 RNA polymerase-mediated *in vitro* transcription to yield a 229-nt probe that contains 34 nt derived from the vector and 195 nt that are complementary to YFV nt 10,520 to 10,714. The RNA probe was purified from a 6% polyacrylamide gel and hybridized overnight at 42°C to 10 μg of total RNA from mock- or YFV-infected BHK cells, using the solutions and protocols supplied with an RPAIII RNase protection assay kit (Ambion). As a positive control, 10 ng of a positive-strand T7 RNA polymerase transcript containing the 3′ 1 kb of the YFV genome was mixed with 10 μg of total BHK cell RNA and treated similarly to the samples containing the YFV- or mock-infected total BHK cell RNA. After hybridization, the samples were treated with RNase A/T1, ethanol precipitated, and subsequently analyzed in a 6% denaturing sequencing gel. A sequence

reaction mix that served as a size marker was run in parallel with the samples in the RNase protection assay.

RNA structure determination by selective 2′-hydroxyl acylation and primer extension (SHAPE) probing. A DNA template containing a T7 RNA polymerase promoter fused to the 3′-terminal 342 nt of YFV was generated by PCR, using *Pfu* DNA polymerase (Fermentas) as described by the manufacturer. The template was digested with EcoRI and HindIII and cloned into pUC9. After linearization with XbaI, the plasmid was used for *in vitro* RNA transcription (T7 MEGAscript kit; Ambion) to obtain a YFV RNA fragment of 188 nt (YFV nt 10,520 to 10,708) for probing of the RNA structure in the region encompassing the predicted RNA pseudoknot (41). RNA was purified as described by the manufacturer (Ambion), and the yield was determined by spectrophotometry.

Probing was performed essentially as previously described (36). Briefly, RNA (20 pmol) in 6 μl H_2O was heated at 95°C for 3 min, cooled down on ice, and subsequently incubated with 3 μl folding buffer at 37°C. After 25 min of incubation, 1 μl of 65 mM *N*-methylisatoic anhydride (NMIA; Sigma) in anhydrous dimethyl sulfoxide (DMSO) was added to the RNA and allowed to react for 60 min at 35°C. The control reaction mixture contained 1 μl of anhydrous DMSO and no NMIA. To determine the NMIA-induced modifications in the 188-bp YFV transcript, 4 pmol (2 μl) of the NMIA-treated RNA was annealed to 10 pM ^{32}P-labeled oligonucleotide 1632 and used for primer extension without any further purification.

RESULTS

Small virus-specific RNAs can be detected in YFV-infected mammalian and insect cells. Recent work (44) demonstrated that cells infected with arthropod-borne flaviviruses produce a small, virus-specific RNA derived from the 3′ UTR. To analyze whether the YFV sfRNA is also produced in infected cells other than BHK-21 cells (44), the mammalian cell lines Vero E6 and SW13 and the mosquito cell line C6/36 were infected with YFV-17D. At 30 h postinfection (p.i.) (mammalian cell lines) or 36 h p.i. (insect cell line), total RNAs were isolated and analyzed by Northern blotting for YFV sfRNA production, using ^{32}P-labeled oligonucleotide 1632, complementary to nt 10,690 to 10,708 in the YFV 3′ UTR, as a probe. Apart from the YFV genomic RNA, three smaller YFV-specific RNAs were detected in the infected mammalian cells (Fig. 1). Using *in vitro* RNA transcripts of various lengths as size markers (data not shown), these RNAs were estimated to be 630 nt (RNA A), 330 nt (RNA B), and 235 nt (RNA C) in length. Based on their estimated sizes and assuming that the RNAs were colinear with the 3′ end of the genome, the 5′ end of RNA A would be located within the carboxy-terminal coding region of NS5, whereas the 5′ ends of RNAs B and C would be in the 3′ UTR. RNA B was the most abundant of these RNAs, and the concentrations of RNA A and RNA C varied depending on the cell line studied. Hardly any RNA A was detected in the infected BHK cells, in which RNA C was relatively abundant, whereas the reverse was true for SW13 cells (Fig. 1, lanes 1 and 3). Surprisingly, RNA B was the only small YFV-related RNA detected in the mosquito cells (C6/36 cells) (Fig. 1). Of the three RNAs detected in the analyzed mammalian cell lines, RNA B appeared to be similar to the recently described YFV sfRNA (44). To keep in line with the nomenclature used in previously published work, RNA B was named sfRNA1. The slightly smaller RNA C was named sfRNA2, which does not imply that this sfRNA is similar to WNV sfRNA2, which can be detected only when the XRN1 stalling site for WNV sfRNA1 is deleted (44).

YFV sfRNA1 and sfRNA2 have identical 5′ ends. Oligonucleotide 1632 (Fig. 2A), which was expected to bind to both sfRNA1 and sfRNA2, was used for primer extension analysis

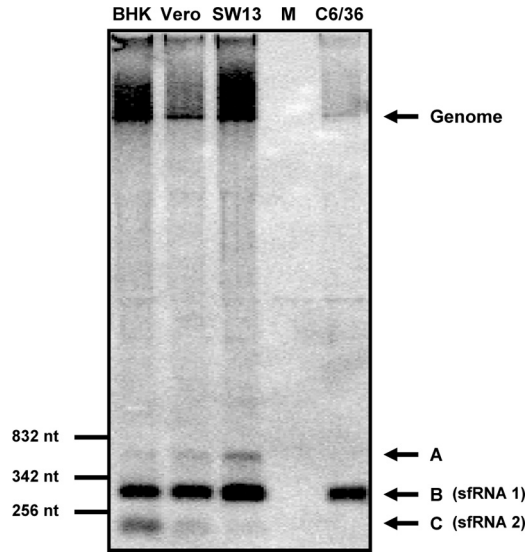

FIG. 1. YFV-17D sfRNA production in mammalian and insect cell lines. The mammalian cell lines BHK-21J, Vero E6, and SW13 and the mosquito cell line C6/36 were infected with YFV-17D at an MOI of 10. At 30 h (mammalian cell lines) or 36 h (mosquito cell line) p.i., total RNA was isolated and analyzed by Northern blotting for the production of YFV-17D sfRNA. Lane M, total RNA isolated from mock-infected BHK-21J cells. Oligonucleotide 1632, complementary to nt 10,690 to 10,708 of the YFV 3′ UTR, was used as a probe. Size markers are indicated on the left. Bands corresponding to the YFV-17D genome and to three small viral RNAs (A, B, and C) are indicated by arrows. RNA B and RNA C are referred to as sfRNA1 and sfRNA2, respectively.

of total RNA isolated from YFV-infected or mock-infected BHK cells. As an additional control, a reaction was performed with a sample containing total RNA of uninfected cells mixed with 1 μg of full-length YFV genome transcript to detect products that resulted from strong stops of the reverse transcriptase on the YFV genome. As shown in Fig. 2B, lane 1, primer extension of oligonucleotide 1632 on total RNA of YFV-infected cells yielded a product that was not present in the RNA of uninfected cells (Fig. 2B, lane 2) or in the sample containing the full-length YFV transcript (Fig. 2B, lane 3). Two primer extension products were observed that differed in size by only one nucleotide. The 5′ ends of these primer extension products were mapped to the A residues at positions 10,532 and 10,533 by use of an oligonucleotide 1632-primed sequence reaction with pBluescript-$YFV_{9845–10861}$ as a size marker. Based on these results, the length of the YFV sfRNA is 329 or 330 nt, which is in agreement with the size estimate for sfRNA1 based on the Northern blots. The result of the primer extension analysis was verified using an RNase protection assay with a gel-purified, ^{32}P-labeled probe that is complementary to 34 nt of the vector and to YFV nt 10,520 to 10,714. This probe has extra YFV nucleotides at the 3′ end relative to the predicted 5′ end of the sfRNA to discriminate between YFV genome and sfRNA protected fragments. As shown in Fig. 2C, some large YFV genome-derived bands were detected in both total RNA of YFV-infected cells and the control sample (Fig. 2C, lanes 2 and 4, respectively). In addition, the probe protected a unique 181- or 182-nt fragment in the total RNA of YFV-infected BHK cells (Fig. 2C, lane 2).

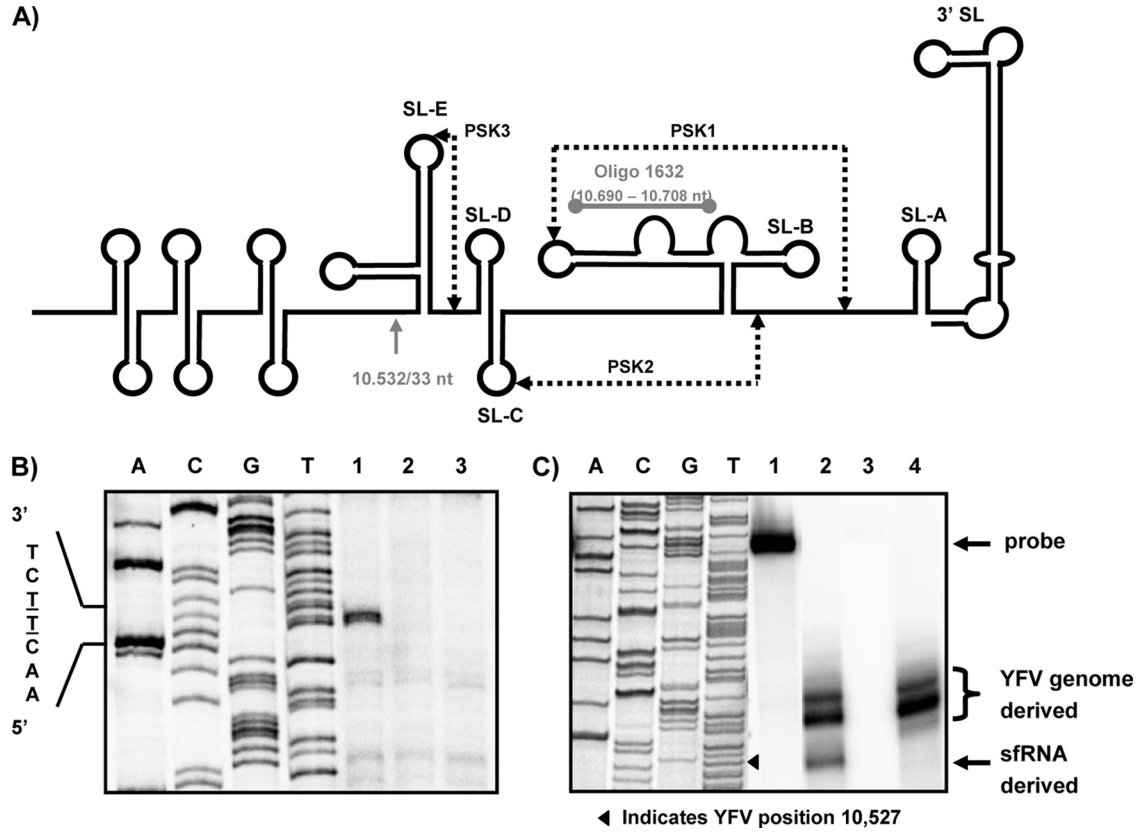

FIG. 2. Determining the 5′ end of the YFV 3′ UTR-specific sfRNAs produced in BHK-21J cells. (A) Schematic diagram of the predicted secondary structure of the YFV 3′ UTR (41). (B) Primer extension analysis using oligonucleotide 1632, which is complementary to YFV nt 10,690 to 10,708 (see panel A). pBluescript-YFV$_{9,845–10,861}$, containing the COOH-terminal part of the YFV NS5 gene and the complete 3′ UTR, was sequenced with oligonucleotide 1632 to obtain a sequencing ladder for determination of the 5′ end of the sfRNAs. Lanes 1 and 2, primer extension on total RNAs isolated from YFV-infected and uninfected BHK-21J cells, respectively; lane 3, primer extension on a full-length *in vitro* YFV transcript mixed with total RNA from uninfected BHK-21J cells. The underlined T residues of the depicted sequence correspond to the 5′ ends of the primer extension products and map the 5′ ends of the YFV sfRNAs to the A residues at positions 10,532 and 10,533 of the YFV genome. (C) RNase protection assay using a 229-nt antisense RNA probe encompassing nt 10,520 to 10,714 of the YFV-17D 3′ UTR. Lane 1, ^{32}P-labeled RNA transcript used as the probe; lane 2, RNA fragments that were protected from RNase digestion after hybridization of the probe to total RNA isolated from YFV-17D-infected cells; lane 3, RNase protection assay on total RNA of mock-infected cells; lane 4, protected RNA fragments obtained when pBluescript-YFV$_{9,845–10,861}$ transcripts mixed with total RNA from mock-infected BHK-21J cells were analyzed. Bands corresponding to the protected fragments derived from either the YFV-17D genome or the sfRNA are indicated. pBluescript-YFV$_{9,845–10,861}$ was sequenced with oligonucleotide 1632 to obtain a marker to determine the sizes of the protected RNA fragments.

The size of the protected RNA fragment agreed with that predicted based on the results of the primer extension analysis and confirmed that the 5′ end of sfRNA1 is at position 10,532 or 10,533.

The most surprising result of these assays was that only these primer extension products and these RNase-resistant RNA fragments were detected, suggesting that sfRNA1 and sfRNA2 have a common 5′ end and that the observed difference in size between the two RNAs was due to a truncation at the 3′ end of sfRNA2. To verify this hypothesis, total RNAs were isolated from YFV-infected BHK-21, Vero E6, SW13, and C6/36 cells and analyzed by Northern blotting, using oligonucleotides 1648 and 1296 as probes. Oligonucleotide 1648 was complementary to nt 10,580 to 10,597 of the YFV genome (Fig. 3A), near the predicted 5′ end of the sfRNAs. Oligonucleotide 1296 should bind to the 3′-terminal 32 nt of the YFV genome (Fig. 3A). As shown in Fig. 3B, oligonucleotide 1648 hybridized to both sfRNA1 and sfRNA2, whereas oligonucleotide 1296 detected only sfRNA1 (Fig. 3C). These results demonstrated that the two YFV sfRNAs have a common 5′ end and that sfRNA2 is indeed truncated at the 3′ end.

YFV sfRNA is generated by the host enzyme XRN1. As recently shown, the host exoribonuclease XRN1 hydrolyzes the WNV genome in a 5′-3′ direction until it is stalled by a currently unknown signal yielding the WNV sfRNA (44). To determine whether XRN1 was also involved in the production of the YFV sfRNAs, the effects of silencing of XRN1 expression on sfRNA production in YFV-infected cells and the *in vitro* production of sfRNA by incubation of YFV transcripts with purified XRN1 were studied. The human-derived SW13 cell line was used in the XRN1 silencing experiments because the nucleotide sequence of the human XRN1 gene is the only one known among the cell lines that were analyzed for YFV sfRNA expression (Fig. 1). SW13 cells were transduced with lentiviruses expressing shRNA direct against the XRN1 transcript or a control shRNA, infected with YFV, and analyzed for XRN1

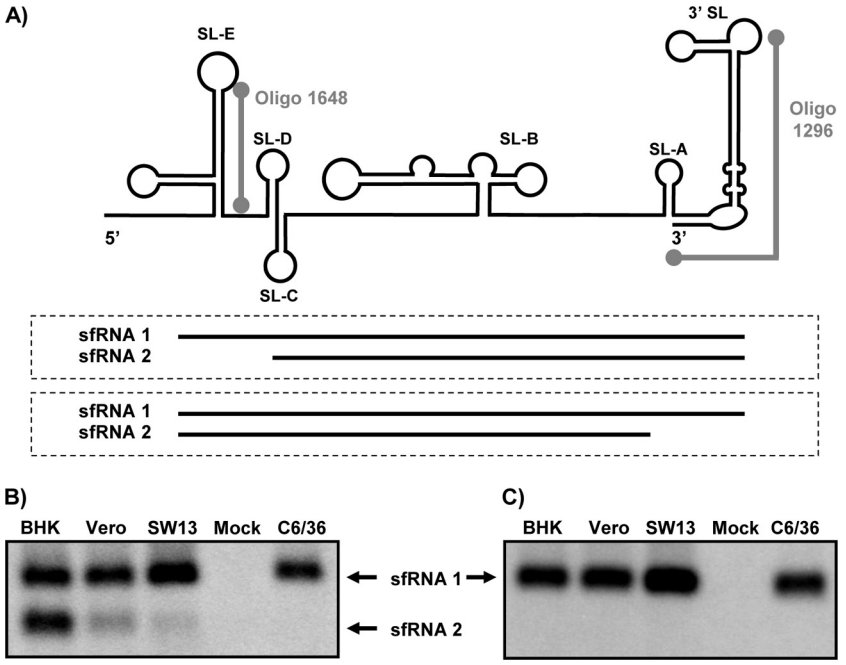

FIG. 3. YFV sfRNA2 is truncated at the 3′ end. (A) Scheme of the YFV 3′ UTR. The two possible orientations of the sfRNAs relative to the YFV 3′ UTR are depicted. The positions of oligonucleotides 1648 and 1296, used to determine the orientations of the sfRNAs, are indicated. Total RNAs were isolated from the indicated YFV-infected cell lines or from mock-infected BHK-21J cells and subsequently analyzed by Northern blotting. (B) Northern blot analysis using oligonucleotide 1648, complementary to YFV-17D nt 10,580 to 10,598. (C) Northern blot analysis using oligonucleotide 1296, complementary to YFV-17D nt 10,830 to 10,862.

expression and YFV sfRNA production by Western and Northern blotting. Expression of each combination of two of the three shRNAs, TRCN-049675, TRCN-049676, and TRCN-049677, in SW13 cells resulted in significantly less production of XRN1 (Fig. 4A, lanes 2, 3, and 4) than that in cells transduced with a similar lentiviral vector expressing a scrambled shRNA (Fig. 4A, lane 1). The silencing of XRN1 expression by the indicated shRNAs was likely specific, since no effect on the expression of actin was observed in these cell lysates (Fig. 4A, bottom panel). As shown by the Northern blot analysis, silencing of XRN1 decreased the production of YFV sfRNA by approximately 90% for all three combinations of shRNAs tested compared to that in cells transduced with a lentivirus expressing a scrambled shRNA (Fig. 4B). The signals for the host cell GAPDH gene were similar in all these lysates, indicating that the observed differences in sfRNA production were not due to significant experimental error. Visual inspection of the cells expressing the shRNAs directed against XRN1 indicated that silencing affected the homeostasis of the cells. This might explain why the hybridization signal for the YFV genome was also somewhat weaker than that in cells transfected with the scrambled shRNA (Fig. 4B).

To determine whether purified XRN1 was able to produce YFV sfRNA *in vitro*, linearized pYF-R.luc2A-RP (25) was used as a template for the production of an uncapped YFV transcript. After treatment with TAP to remove the XRN1-blocking 5′-triphosphate, this RNA was incubated with 0.1 or 1 unit of XRN1 and analyzed by Northern blot analysis for sfRNA production. Incubation of YF-R.luc2A-RP RNA with XRN1 resulted in the production of a small YFV-specific RNA that comigrated with the sfRNA1 produced in YFV-infected BHK-21J cells (Fig. 5A). Primer extension analysis was performed to provide additional evidence that this small RNA produced *in vitro* truly reflected the YFV sfRNA. As shown in Fig. 5B, primer extension using oligonucleotide 1632 resulted in similarly sized products for both XRN1-treated YF-R.luc2A-RP RNA transcript and total RNA from YFV-infected BHK cells. The fact that the smaller sfRNA2 was readily detectable in YFV-infected BHK-21J cells and not in the *in vitro* XRN1 assays is in line with our previous findings that sfRNA1 and sfRNA2 have a common 5′ end and suggests that additional RNA processing is required to yield sfRNA2.

From the results obtained with the RNA silencing experiments and the *in vitro* YFV sfRNA production by purified XRN1, it was concluded that similar to the case for WNV, the host RNase XRN1 is responsible for the production of YFV sfRNAs.

An RNA pseudoknot in the YFV 3′ UTR is required for production of sfRNAs. Compared to the predicted RNA structure of the YFV 3′ UTR (41), the 5′ end of sfRNA1 and sfRNA2 is located just a few nucleotides upstream of SL-E (Fig. 2A), which is part of an RNA pseudoknot. To determine whether the predicted RNA structures that form this pseudoknot (PSK3) are required for YFV sfRNA production, site-directed mutagenesis was used to construct pACNR-FLYF-17DΔSL-E, which lacked nt 10,537 to 10,596 (which form SL-E) and was therefore unable to form PSK3. *In vitro*-transcribed RNA of AflII-linearized pACNR-FLYF-17DΔSL-E was electroporated into BHK-21J cells that were subsequently analyzed for viral RNA replication by [^{3}H]uridine labeling and for sfRNA synthesis by Northern blotting. Despite the relatively minor effects on viral replication (Fig. 6A), no YFV sfRNA could be de-

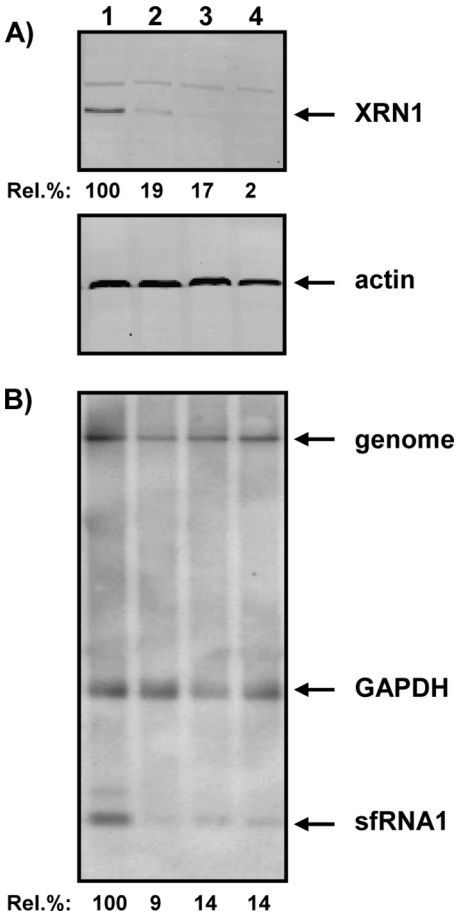

FIG. 4. shRNA-mediated XRN1 silencing decreases YFV sfRNA production. SW13 cells were transduced with an shRNA-expressing lentivirus from the MISSIONTRC-Hs1.0 library (Sigma) and then infected with YFV-17D as described in Materials and Methods. Lentiviruses expressed the following shRNAs: lane 1, scrambled shRNA (SHC-002); lane 2, shRNAs TRCN-049675 and TRCN-049676; lane 3, shRNAs TRCN-049675 and TRCN-049677; and lane 4, shRNAs TRCN-049676 and TRCN-049677. (A) XRN1 and actin expression in Western blots. Rel. %, percentage of XRN1 expression in cells transduced with shRNAs against XRN1 compared to that in cells expressing the scrambled shRNA. (B) YFV sfRNA production and GAPDH mRNA expression by Northern analysis. Rel. %, expression of YFV sfRNA in cells transduced with shRNAs against XRN1 compared to that in cells expressing the scrambled shRNA.

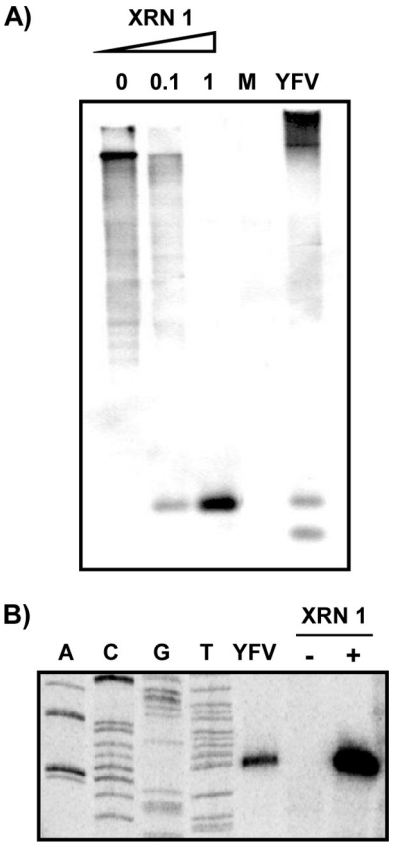

FIG. 5. *In vitro* production of YFV-17D sfRNAs by the host exoribonuclease XRN1. TAP-treated *in vitro* RNA transcripts of YF-R.luc2A-RP were incubated with the indicated units of XRN1 and analyzed by hybridization after denaturing gel electrophoresis (A) and primer extension (B), using oligonucleotide 1632, complementary to YFV-17D nt 10,690 to 10,708, as a probe and primer, respectively. RNAs isolated from mock (M)- and/or YFV-infected BHK-21J cells were used as controls in both experiments.

tected in the cells transfected with YFV-ΔSL-E RNA (Fig. 6B). To demonstrate that the lack of sfRNA production in the cells transfected with YFV-ΔSL-E RNA was due to disruption of the XRN1 stalling site, transcripts of this mutant were incubated *in vitro* with purified XRN1. As shown in Fig. 6C, XRN1 was not stalled when SL-E was deleted and therefore no sfRNA was produced. These *in vitro* and *in vivo* results together demonstrate that SL-E encompasses RNA structures and/or sequences that are essential for stalling XRN1 and therefore for YFV sfRNA production. The YFV-ΔSL-E mutant virus was delayed in inducing CPE in BHK cells. It also showed a slight delay in initial virus production but reached a similar maximum titer to that of the parental virus (Fig. 6D).

Two sets of additional mutants were constructed to dissect the role of SL-E in YFV sfRNA synthesis in more detail. The first set of mutants focused on the role of the top stem structure of SL-E (referred to as e2) (41). In mutant YFV-e2AA, the right arm of the stem (5′-GCAGU-3′; YFV nt 10,583 to 10,587) was replaced by the sequence of the left part of the stem (5′-ACUGC-3′) (Fig. 7A). Due to these mutations, the formation of SL-E e2 was expected to be disrupted. YFV-e2BB was the opposite of the YFV-e2AA mutant. In this mutant, the left part of the e2 stem (5′-ACUGC-3′; YFV nt 10,567 to 10,571) was replaced by the nucleotide sequence of the right arm of SL-E e2 (5′-GCAGU-3′) (Fig. 7A). In the YFV-e2BA mutant, the possibility to form stem e2 was restored by switching the parental YFV-17D original sequences of the left and right arms of the stem. BHK-21J cells were electroporated with *in vitro*-transcribed RNAs of the parental YFV-17D strain and the YFV-e2 stem mutants. Cells were analyzed for genome RNA synthesis by [^{3}H]uridine labeling and for sfRNA production by Northern blotting with oligonucleotide 1632. As shown in Fig. 7B, all three YFV-e2 mutants were able to synthesize viral genomic RNA efficiently. Strikingly, neither YFV-e2AA nor YFV-e2BB was able to produce detectable amounts of sfRNA (Fig. 7C). Restoring the possibility to form stem e2, as in YFV-e2BA, also restored the

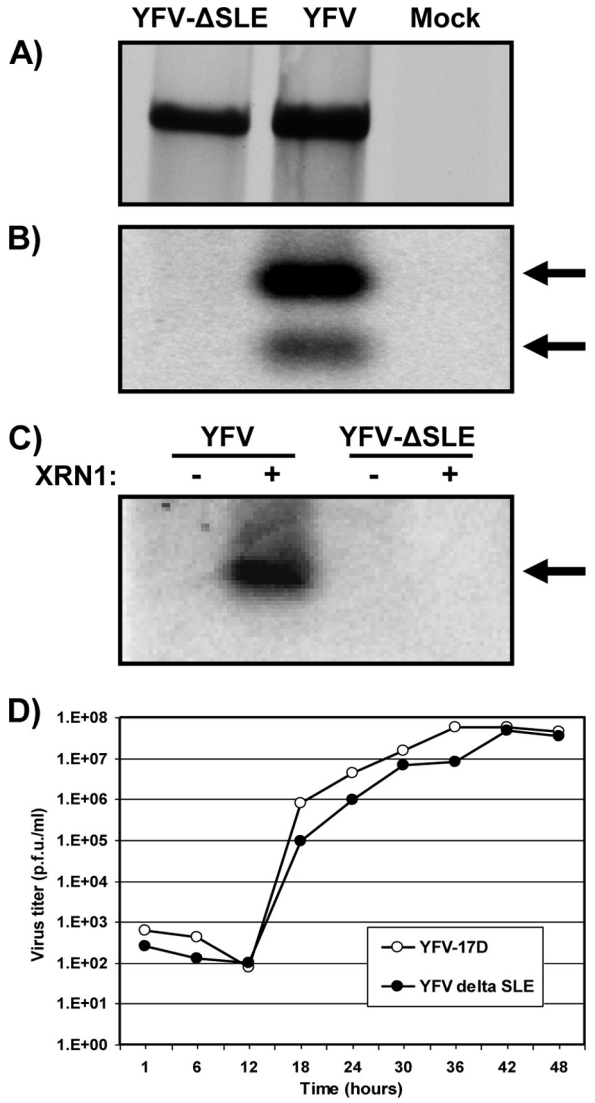

FIG. 6. Stem-loop structure SL-E in the YFV 3′ UTR is required for the production of sfRNA. (A) Viral RNA synthesis in BHK-21J cells transfected with *in vitro*-transcribed genome-length RNAs of YFV-17D and YFV-ΔSL-E. Transfected cells were labeled with [^{3}H]uridine from 18 to 24 h posttransfection. Total RNAs were isolated and analyzed after denaturation by agarose gel electrophoresis, as described in Materials and Methods. (B) sfRNA production in BHK-21J cells transfected with YFV-17D and YFV-ΔSL-E transcripts. Total RNAs were isolated at 24 h posttransfection and analyzed by Northern blotting and hybridization with oligonucleotide 1632 (complementary to YFV-17D nt 10,690 to 10,708). The sfRNAs are indicated by arrows. (C) *In vitro* RNA transcripts of YFV-17D and YFV-ΔSL-E were incubated in the presence or absence of 1 unit of XRN1 and analyzed for the production of sfRNA by Northern blotting, using oligonucleotide 1632 as a probe. The sfRNA is indicated by an arrow. (D) Viral growth kinetics of YFV-17D and the YFV-ΔSL-E mutant. BHK-21J cells were infected at an MOI of 5, and the medium of the infected cells was sampled at the indicated times postinfection. Titers were determined by plaque assays on BHK-21J cells.

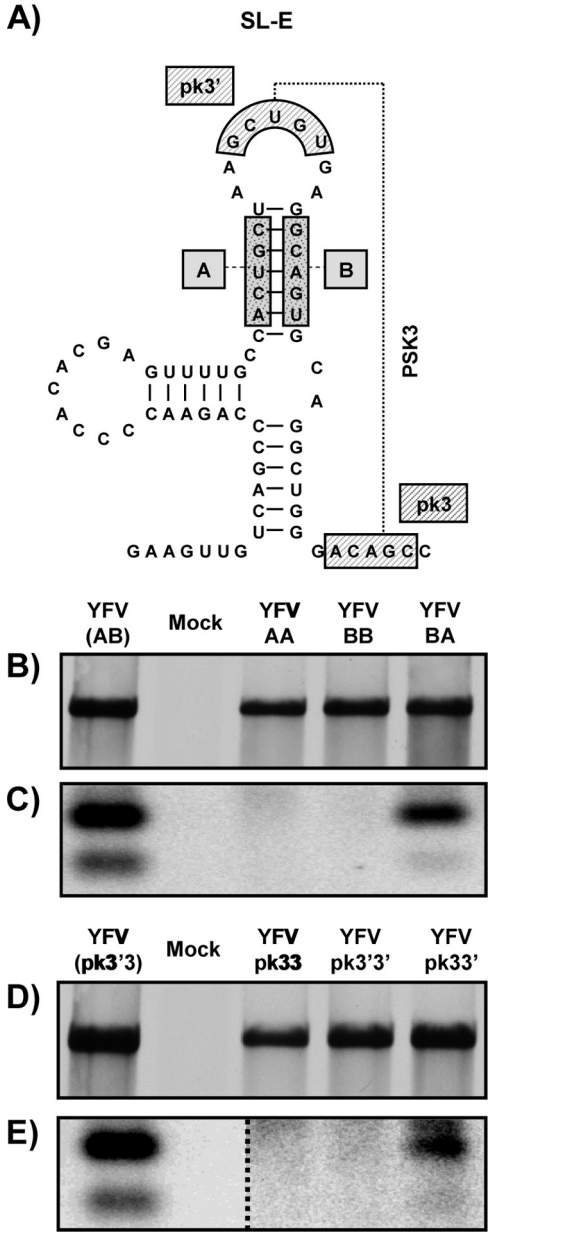

FIG. 7. YFV-17D RNA pseudoknot 3 is required for sfRNA production. (A) Schematic diagram of the YFV 3′ UTR SL-E structure. The primary sequences involved in stem-loop e2 (sequences A and B) and in the pseudoknot interaction (sequences pk3′ and pk3) are depicted. (B and D) Viral RNA synthesis in BHK-21J cells transfected with *in vitro*-transcribed genomic RNAs of YFV-17D and YFV mutant viruses (at SL-E e2 [B] and at PSK3 [D]). Transfected cells were labeled with [^{3}H]uridine from 18 to 24 h posttransfection. Total RNAs were isolated and analyzed after denaturation by agarose gel electrophoresis, as described in Materials and Methods. YFV(AB) and YFV(pk3′3) indicate wild-type YFV-17D for these different groups of mutants. (C and E) Northern blot analysis of RNAs isolated from BHK cells 30 h after transfection with YFV-17D and YFV mutant viruses (at SL-E e2 [C] and at PSK3 [E]). Oligonucleotide 1632 (complementary to YFV-17D nt 10,690 to 10,708) was used as a probe. In panel E, the dotted line separates the wild-type YFV-17D and mock lanes from the same Northern blot at a higher exposure.

production of YFV sfRNA. Although in comparison to YFV-17D YFV-e2BA produced less sfRNA, both viruses induced CPE in the cells about 48 h after electroporation, whereas YFV-e2AA and YFV-e2BB were clearly delayed in CPE in-

duction compared to the parental virus. The kinetics of virus production in BHK-21 cells were similar to that shown for YFV-ΔSL-E (e.g., YFV-e2AA) or closer to that for the parental virus (data not shown). The fact that the YFV sfRNAs were produced in cells infected with YFV-e2BA indicated that the SL-E structure was more important than the primary sequence for producing the sfRNA.

SL-E is predicted to be part of a more complex RNA structure in which the sequence 5′-GCUGU-3′ (pk3′; YFV nt 10,575 to 10,579) in the top loop of e2 is predicted to base pair with the sequence 3′-CGACA-5′ (pk3; YFV nt 10,598 to 10,602) immediately downstream of SL-E, forming an RNA pseudoknot (PSK3) (Fig. 7A) (41). A second set of YFV mutants was constructed to determine whether the pk3′-pk3 interaction is important for YFV sfRNA production. In YFV-pk3′pk3′ and YFV-pk3pk3, the downstream pk3 sequence or the upstream pk3′ sequence was replaced by the complementary sequence. For both of these mutants, PSK3 formation was expected to be disrupted. In YFV-pk3pk3′, the possibility to form PSK3 was restored, albeit with the positions of the pk3′ and pk3 sequences reversed in comparison to those in YFV-17D. [^{3}H]uridine labeling of BHK cells transfected with *in vitro*-transcribed full-length RNAs of these mutants demonstrated that they replicated quite efficiently (Fig. 7D). More importantly, no sfRNA could be detected in cells transfected with YFV-pk3′pk3′ or YFV-pk3pk3, whereas YFV sfRNA could be detected in cells electroporated with the YFV-pk3pk3′ mutant, in which the ability to form PSK3 was restored (Fig. 7E). However, the amount of sfRNA produced by YFV-pk3pk3′ was far less than that observed for the parental YFV-17D strain and required contrast enhancement of the phosphorimager data, which changed only the view of the data, not the data themselves. All three pk3-pk3′ mutant viruses showed a significant delay in the onset of CPE in BHK cells compared to YFV-17D. The kinetics of virus production in BHK-21 cells were similar to that for YFV-17D, except for YFV-pk3′pk3′, whose kinetics was like that of YFV-ΔSL-E (data not shown).

The combined results of the mutagenesis of the SL-E e2 stem and the pk3′-pk3 sequences strongly suggest that the predicted H-type RNA pseudoknot PSK3 is required to stall XRN1, resulting in the production of YFV sfRNA.

Insertion of the PSK3 sequence into a heterologous RNA results in production of an sfRNA-like RNA. The fact that the base pairings in SL-E stem e2 and between pk3′ and pk3 are important determinants of YFV sfRNA synthesis did not exclude the possibility that this region is part of a more complex RNA structure, including additional elements downstream of PSK3. To address this possibility, a synthetic MluI-SphI DNA mimicking YFV nt 10,521 to 10,662 and YFV nt 10,531 to 10,611 was inserted into a Sinrep5 vector (6) that contained an enhanced green fluorescent protein (GFP) gene just upstream of the insertion site (Fig. 8A). This resulted in two constructs: pSinrep5-eGFP-YFV$_{10,521–10,662}$, encoding the SL-E to SL-C fragment of the YFV 3′ UTR; and pSinrep5-eGFP-YFV$_{10,531–10,611}$, encoding the YFV SL-E/PSK3 region. The GFP gene allowed for easy determination of the transfection efficiency and for discrimination between the Sindbis virus subgenomic RNA and a potentially produced sfRNA-like RNA. BHK-21J cells were transfected with *in vitro*-transcribed RNAs of the Sinrep5-eGFP and Sinrep5-eGFP-YFV mutants. RNAs were isolated at 8 h p.e. and analyzed for sfRNA-like RNA production by Northern blotting and hybridization, with two oligonucleotides as probes. Probe 1674 was complementary to nt 7,601 to 7,625 of Sindbis virus and was expected to hybridize to both the Sinrep5 genomic and subgenomic mRNAs, whereas probe 1648, which was complementary to YFV SL-E (nt 10,580 to 10,597), was expected to hybridize not only to Sinrep5 mRNAs but also to any sfRNA-like RNA produced in the transfected cells. As shown in Fig. 8B, hybridization of total RNA of the transfected cells with oligonucleotide 1674 demonstrated that Sinrep5-eGFP and both Sinrep5-eGFP-YFV$_{10,521–10,622}$ and pSinrep5-eGFP-YFV$_{10,531–10,611}$ replicated efficiently and produced a subgenomic mRNA of the expected size in the transfected BHK cells. In addition to the recombinant Sinrep5 genomic and subgenomic mRNAs, hybridization with oligonucleotide 1648 revealed the production of an additional small RNA that was unique for the cells transfected with Sinrep5-eGFP-YFV$_{10,521–10,662}$ and pSinrep5-eGFP-YFV$_{10,531–10,611}$ (Fig. 8B, lanes 6 and 7). The size of this RNA was in agreement with what was expected for the production of an sfRNA-like RNA in pSinrep5-eGFP upon insertion of the YFV sequences. Primer extension of total RNAs from cells transfected with Sinrep5-eGFP-YFV$_{10,521–10,662}$ and pSinrep5-eGFP-YFV$_{10.531–10.611}$ (Fig. 8C) showed that the 5′ end of the sfRNA-like RNA produced in these transfected cells was similar to that of the sfRNA produced in YFV-infected cells. Taken together, these results clearly demonstrate that YFV nt 10,531 to 10,611, containing the region that allows the formation of PSK3, are sufficient to stall XRN1. Furthermore, these results also indicate that RNA structures downstream of PSK3 are not required for the production of sfRNA.

Chemical RNA probing provides evidence of the formation of PSK3. To obtain additional evidence to support the formation of PSK3, *in vitro* structure probing by SHAPE with NMIA (36) was performed on an *in vitro*-synthesized RNA template containing YFV 3′ UTR nt 10,520 to 10,708, encompassing PSK3. As shown in Fig. 9B, chemical probing of this region of the wild-type YFV-17D genome essentially confirmed the previously predicted RNA structure model (41). Apart from the nucleotides predicted to form the top loop of the side stem SL-E e3 (Fig. 9A), most of the other nucleotides did not react with NMIA, indicating that they were in a double-stranded conformation. This observation also includes the nucleotides of the pk3′ and pk3 sequences (Fig. 9B). The lack of reactivity to NMIA of these particular sequences was in agreement with the prediction that these complementary sequences could base pair to form the PSK3 pseudoknot.

The mutants that should have disrupted (YFV-pk3′pk3′ and YFV-pk3pk3) or restored (YFV-pk3pk3′) PSK3 formation were also subjected to RNA structure probing. The NMIA reactivity patterns of these mutant RNAs showed that the overall SL-E structure was maintained but that especially the pk3′ sequence, and to a somewhat lesser extent the pk3 sequence, were now susceptible to modification by NMIA (Fig. 9B), indicating that these sequences were no longer base pairing to form PSK3. Surprisingly, a similar result was also obtained for the putatively restored YFV-pk3pk3′ mutant RNA, indicating that despite the nucleotide complementarity be-

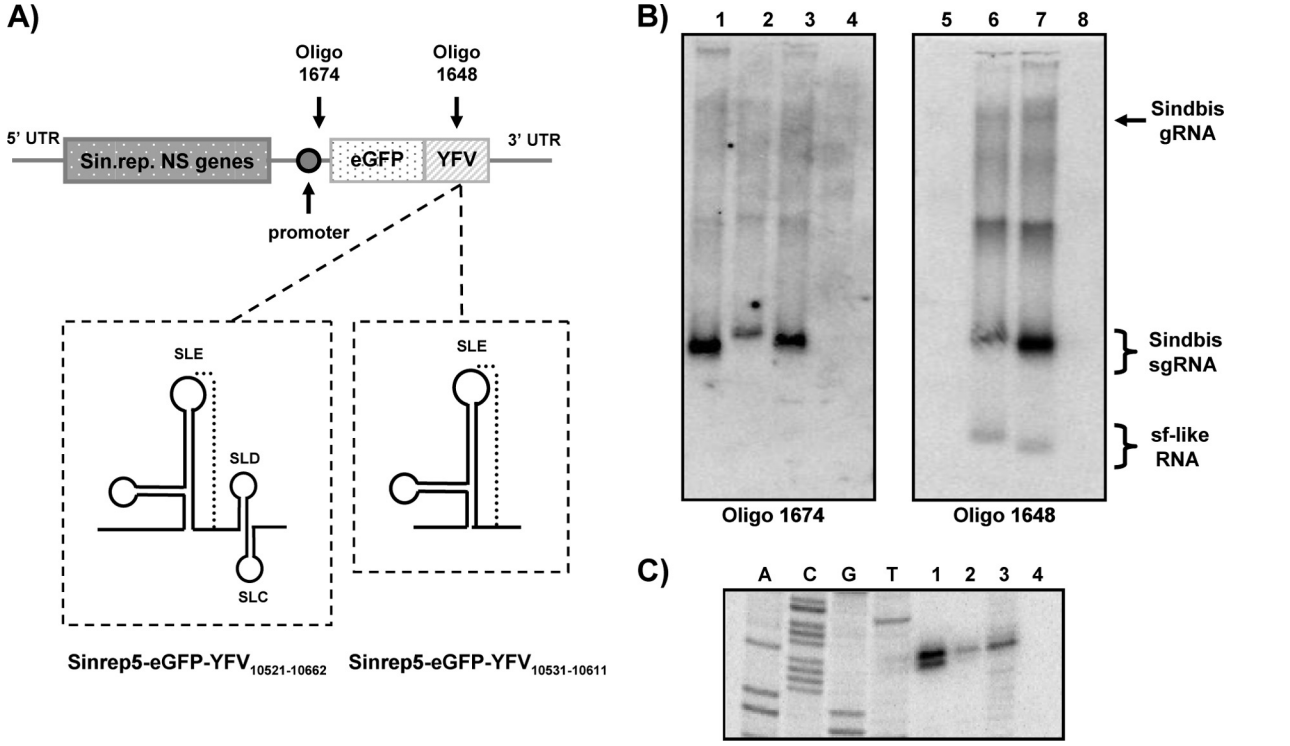

FIG. 8. Insertion of sequences required for the formation of PSK3 is sufficient to produce an sfRNA-like RNA in the context of a Sindbis virus replicon. (A) Scheme of the characteristics of the pSinrep5 vector and the predicted structures of the YFV-17D regions that were inserted into the vector. The YFV 3′ UTR nucleotides cloned into pSinRep5-eGFP are indicated in the name of each construct. The promoter for the enhanced GFP (eGFP)-expressing subgenomic Sinrep mRNA and the binding sites for oligonucleotides 1674 and 1648 are indicated. (B) Northern blot analysis of RNAs isolated from BHK-21J cells at 8 h p.e. with Sinrep5-eGFP (lanes 1 and 5), Sinrep5-eGFPYFV$_{10,521–10,662}$ (lanes 2 and 6), and Sinrep5-eGFPYFV$_{10,531–10,611}$ (lanes 3 and 7) RNAs; lanes 4 and 8 correspond to uninfected BHK-21J cells. Oligonucleotide 1674 and oligonucleotide 1648 were used as probes, as specified in the figure. The Sindbis virus genomic (gRNA) and subgenomic (sgRNA) RNAs and the sfRNA-like RNAs are indicated. (C) Primer extension analysis with oligonucleotide 1648 to determine the 5′ end of the sfRNA-like RNAs produced with the Sinrep5 mutants. pBluescript-YFV$_{9,845–10,861}$ was sequenced with oligonucleotide 1648 to obtain a sequencing ladder. RNAs isolated from BHK-21J cells transfected with YFV-17D (lane 1), Sinrep5-eGFPYFV$_{10,521–10,662}$ (lane 2), and Sinrep5-eGFPYFV$_{10,531–10,611}$ (lane 3) were analyzed; lane 4 corresponds to mock-transfected cells.

tween the pk3 and pk3′ sequences, the formation of PSK3 was not restored in this mutant.

Nonetheless, the structural probing data obtained with the RNA fragment encompassing YFV-17D nt 10,520 to 10,708 provided strong support for the previously proposed structural model (41).

DISCUSSION

The generally accepted concept that the viral genome, which also serves as the viral mRNA, and the genome-length, minus-strand RNA are the only RNA species that can be detected in cells infected with flaviviruses was recently challenged. Several studies have now shown that in addition to these genome-length viral RNAs, a small, positive-strand viral RNA (sfRNA) is produced in cells infected with arthropod-borne flaviviruses (29, 31, 44, 49, 56). Recently, the sfRNA was shown to be a product of incomplete 5′-to-3′ degradation of the viral genome by the host exoribonuclease XRN1 and to serve as an important determinant of viral pathogenicity (44). This study describes the production of sfRNA by XRN1 in YFV-infected cells and, more importantly, defines an RNA pseudoknot in the viral 3′ UTR as a prerequisite for stalling of XRN1, resulting in the production of the sfRNA.

Not one but two sfRNAs are detected in YFV-infected cells. Another, larger YFV-specific RNA was also detected in infected mammalian cell lines, especially in SW13 cells. This RNA is likely an instable intermediate of 5′-to-3′ XRN1-mediated decay of the viral genome. Silencing of XRN1 in YFV-infected SW13 cells resulted in a significant decrease of YFV sfRNA1 as well as the larger YFV-specific RNA A. Digestion of YFV genome transcripts with purified XRN1 resulted in the *in vitro* production of sfRNA1, providing the ultimate proof for the role of XRN1 in YFV sfRNA production.

Mapping of the positions of sfRNA1 and sfRNA2 in the 3′ UTR of the YFV genome revealed that sfRNA1 was colinear with the distal part of the 3′ UTR. Both sfRNAs had the same 5′ end, and the smaller size of sfRNA2 was due to a truncation at the 3′ end. sfRNA2 was never detected upon *in vitro* digestion of YFV genome transcripts with purified XRN1. One hypothesis that could explain this truncation is that sfRNA2 is derived by XRN1 digestion of a YFV genomic RNA template that is already truncated at the 3′ end. Alternatively, sfRNA2 could be the result of additional processing by an exo- or

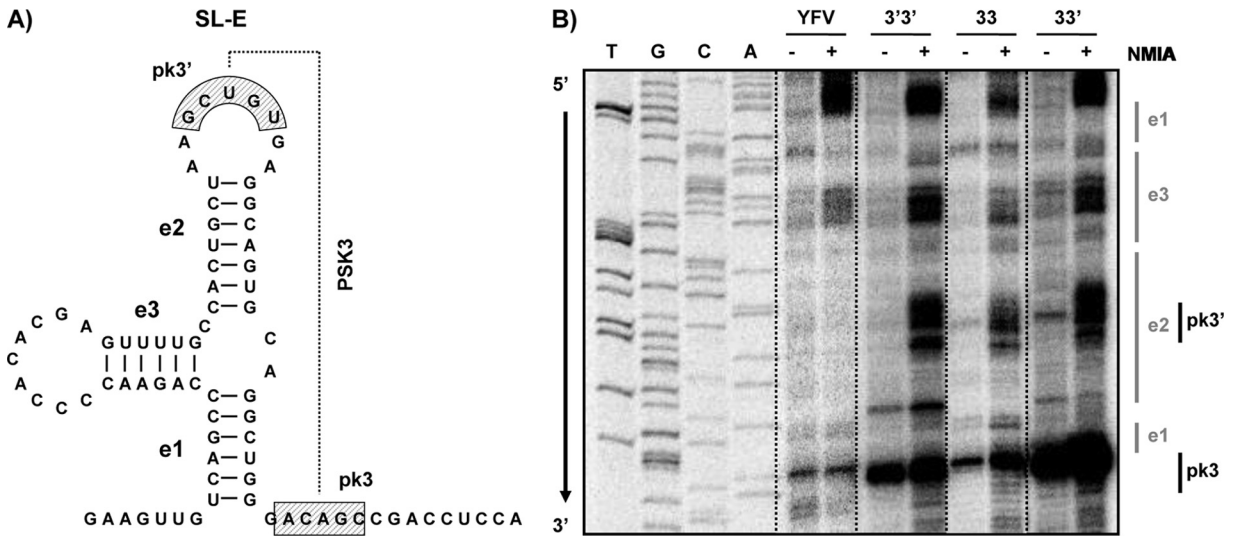

FIG. 9. The predicted pseudoknot PSK3 at the wild-type YFV 3′ UTR is genuine. (A) Schematic diagram of the minimal YFV 3′ UTR region (nt 10,531 to 10,611) required for stalling of XRN1. Sequences involved in the pseudoknot interaction are depicted. (B) *In vitro* structure probing by SHAPE with wild-type YFV and the PSK3 mutants YFV-pk3′pk3′, YFV-pk3pk3, and YFV-pk3pk3′. After treatment with NMIA, which preferentially reacts with bases in a single-stranded conformation, *in vitro*-synthesized RNA templates (YFV nt 10,520 to 10,708) were analyzed by primer extension with oligonucleotide 1632 (complementary to YFV nt 10,690 to 10,708). Samples were treated with either 65 mM NMIA in DMSO (+) or, as a control, DMSO only (−). The different substructures of SL-E and the pk3 and pk3′ sequences are indicated on the right relative to their positions in the NMIA reactivity pattern. pBluescript-$YFV_{9,845–10,861}$ was sequenced with oligonucleotide 1632 to obtain a sequencing ladder.

endoribonuclease at the 3′ end of sfRNA1. Currently, we have no evidence to favor one of these hypotheses. Interestingly, it has been shown that in insect cells the 5′-to-3′ decay pathway is the dominant route for overall RNA turnover (5), while in mammalian cells the relative contributions of 5′-to-3′ and 3′-to-5′ RNA degradation pathways to RNA turnover are still a subject of debate (reviewed in reference 21). The fact that sfRNA2 was not detected in infected mosquito cells thus supports the hypothesis that sfRNA2 is the result of 3′-to-5′ processing.

Both the primer extension and RNase protection assays mapped the 5′ end of the YFV sfRNAs to nucleotide 10,532 or 10,533, which is just upstream of a predicted H-type RNA pseudoknot (PSK3) (41) that includes SL-E. The inability of XRN1 to produce an sfRNA both *in vivo* and *in vitro* when SL-E was disrupted strongly indicates that this region contains essential elements for the stalling of this host RNase. XRN1 can be blocked by elements such as strong secondary structures or G-track sequences (15, 18, 38, 58). The YFV PSK3 region is not particularly G rich but adopts a complex RNA structure. So far, no experimental evidence supporting the formation of PSK3 has been presented, nor has this structure been implicated in any biologically relevant function. Our RNA structure probing of the PSK3 region provided unequivocal evidence of the presence of this RNA pseudoknot in the YFV 3′ UTR. Disruption of the SL-E structure resulted in viruses that replicated with a similar efficiency to that of YFV-17D but did not produce detectable amounts of sfRNA. Reconstituting the SL-E structure in a YFV mutant, albeit with different base pairs, resulted in sfRNA production in cells infected with this mutant. On the other hand, disrupting the predicted PSK3 resulted in mutant viruses that replicated efficiently but were no longer able to produce sfRNA. Surprisingly, when the base pairing possibility was restored (YFV-pk3pk3′), sfRNA production was hardly detectable. These data are supported by the probing results showing that although the overall SL-E structure was maintained in all PSK3 mutants, none of them showed any significant base pairing of the nucleotides involved in the equivalent of the parental pk3′-pk3 interaction. Although restoration of the pseudoknot was expected in the YFV-pk3pk3′ mutant, this seemed to occur in only a minor fraction of the RNA molecules, which explains why they were not detected in the probing experiments and why enhancement of the contrast in the picture of the Northern blot was required. The experiments using the Sinrep5 expression system demonstrated that YFV nt 10,531 to 10,611, predicted to form PSK3, contain all of the RNA sequences and structures that are needed to stall XRN1. In an attempt to restore PSK3 interaction and subsequent sfRNA production, an additional YFV mutant was constructed in which the pk3′ and pk3 sequences were replaced by 5′-CCCGC-3′ and 5′-GCGGG-3′ sequences, respectively, to enhance the thermodynamic stability of this interaction. Although this mutant was viable, it did not produce any sfRNA (data not shown), and probing provided no evidence of a pk3′-pk3 interaction (data not shown). Taken together, our mutational analysis and probing results support the actual formation of PSK3 in the 3′ UTR of YFV but also indicate that the formation of this pseudoknot is sequence dependent. For many viral pseudoknots, the primary sequence is unimportant for function, as long as the conformation and overall stability of the structure are maintained (reviewed in reference 8). Nonetheless, there are other pseudoknots in which subtle nucleotide changes interfere with pseudoknot thermodynamic stability and are deleterious for pseudoknot function (14, 40). Examples of viruses in which the primary sequence proved to be important for RNA pseudoknot stability and/or function

include tobacco mosaic virus (27), beet western yellow virus (55), severe acute respiratory syndrome (SARS) coronavirus (4, 45), and Visna-Maedi virus (43). A similar situation can also be envisioned for YFV, in which specific constraints to sustain the overall stability/conformation of the higher-order RNA structure of PSK3 can be fulfilled only by the wild-type sequence. The fact that the pk3′ and pk3 sequences are well conserved among the different YFV strains (9, 39) supports this idea. The observation that disruption of PSK3 allows XRN1 to degrade the viral genome completely implies that the YFV genome has one unique stalling site for XRN1 within the 3′ UTR. This observation differs from the case for KUNV, in which more than one stalling site was found (44).

It was shown that KUNVs deficient in sfRNA production are significantly more attenuated in cell culture and in mice than viruses that produce the sfRNA, suggesting an important role for the sfRNA in viral pathogenicity (44). A similar observation was made with our YFV mutants: viruses that were unable to produce sfRNA were also unable to form plaques on SW13 cells, despite the fact that they were able to replicate efficiently in these cells (data not shown). Interestingly, it has previously been hypothesized that there is a correlation between the structure of the YFV region predicted to form PSK3 and the degree of virulence exhibited by the virus (46). Although these observations for KUNV and YFV may hint at a function of the sfRNA, it is still unclear how sfRNA synthesis relates to viral pathogenesis. It has been suggested that the sfRNA could modulate the host antiviral responses by antagonizing or inactivating certain cellular RNA sensors (e.g., TLR3, RIG-I, and MDA5) or that it could act as a decoy for cellular microRNAs (20). Since KUNV sfRNA was reported to be generated by XRN1 in P bodies (44), and since these P bodies contain, besides 5′-3′ degradation components, proteins involved in translational repression, mRNA surveillance, and RNA-mediated gene silencing (reviewed in references 2, 19, 21, and 42), one could speculate that the sfRNA could indeed be involved in a pathway linked to P bodies, such as RNA-mediated gene silencing. However, a progressive decrease in the number of P bodies during the time course of DENV-2 and WNV infections of BHK cells has been reported (17). Alternatively, either free in the cytoplasm or associated with cellular structures, the sfRNA could also act as a decoy to sequester a host protein(s) that would otherwise bind to the genomic 3′ UTR and exert a negative effect on the virus.

Additional studies are needed to determine the kinetics of sfRNA production, its subcellular localization, and potential sfRNA-interacting host factors. Previous studies with flaviviruses containing mutations or deletions in the genomic 3′ UTR region should be reevaluated in light of the potential effect of such mutations on the production and function of the sfRNA. For instance, deletions involving the SL-II region of DENV (which is comparable to the YFV SL-E) that resulted in restricted growth in cell culture, different plaque phenotypes, and viral attenuation (1, 35) could be explained by the lack of sfRNA production, illustrating the importance of the sfRNA in viral pathogenesis.

From this study and those of others, it is obvious that a simple deletion that disrupts the stalling site for XRN1 may be used to construct attenuated flaviviruses that could be considered vaccine candidates. However, it remains to be established whether the reduced pathogenicity of sfRNA-deficient viruses interferes with the broad immune response that is required to induce protection against wild-type virus infection or, even worse, results in persistent infections after administration of the vaccine.

ACKNOWLEDGMENTS

We thank M. Rabelink and R. C. Hoeben for technical advice and support in preparing the lentiviruses for the XRN1 RNA silencing experiments and X. Jiang for providing the GAPDH cDNA fragment that was used to generate a GAPDH probe in the analysis of the XRN1 RNA silencing experiments.

REFERENCES

1. **Alvarez, D. E., A. L. De Lella Ezcurra, S. Fucito, and A. V. Gamarnik.** 2005. Role of RNA structures present at the 3′UTR of dengue virus on translation, RNA synthesis, and viral replication. Virology **339:**200–212.
2. **Anderson, P., and N. Kedersha.** 2006. RNA granules. J. Cell Biol. **172:**803–808.
3. **Ausubel, F. M., R. Brent, R. E. Kingston, D. D. Moore, J. G. Seidman, J. A. Smith, and K. Struhl.** 2000. Current protocols in molecular biology. Wiley Interscience, New York, NY.
4. **Baranov, P. V., C. M. Henderson, C. B. Anderson, R. F. Gesteland, J. F. Atkins, and M. T. Howard.** 2005. Programmed ribosomal frameshifting in decoding the SARS-CoV genome. Virology **332:**498–510.
5. **Bonisch, C., C. Temme, B. Moritz, and E. Wahle.** 2007. Degradation of hsp70 and other mRNAs in Drosophila via the 5′ 3′ pathway and its regulation by heat shock. J. Biol. Chem. **282:**21818–21828.
6. **Bredenbeek, P. J., I. Frolov, C. M. Rice, and S. Schlesinger.** 1993. Sindbis virus expression vectors: packaging of RNA replicons by using defective helper RNAs. J. Virol. **67:**6439–6446.
7. **Bredenbeek, P. J., E. A. Kooi, B. Lindenbach, N. Huijkman, C. M. Rice, and W. J. Spaan.** 2003. A stable full-length yellow fever virus cDNA clone and the role of conserved RNA elements in flavivirus replication. J. Gen. Virol. **84:**1261–1268.
8. **Brierley, I., S. Pennell, and R. J. Gilbert.** 2007. Viral RNA pseudoknots: versatile motifs in gene expression and replication. Nat. Rev. Microbiol. **5:**598–610.
9. **Bryant, J. E., P. F. Vasconcelos, R. C. Rijnbrand, J. P. Mutebi, S. Higgs, and A. D. Barrett.** 2005. Size heterogeneity in the 3′ noncoding region of South American isolates of yellow fever virus. J. Virol. **79:**3807–3821.
10. **Cheng, C. P., E. Serviene, and P. D. Nagy.** 2006. Suppression of viral RNA recombination by a host exoribonuclease. J. Virol. **80:**2631–2640.
11. **Chu, P. W., and E. G. Westaway.** 1985. Replication strategy of Kunjin virus: evidence for recycling role of replicative form RNA as template in semiconservative and asymmetric replication. Virology **140:**68–79.
12. **Cleaves, G. R., T. E. Ryan, and R. W. Schlesinger.** 1981. Identification and characterization of type 2 dengue virus replicative intermediate and replicative form RNAs. Virology **111:**73–83.
13. **Cook, S., and E. C. Holmes.** 2006. A multigene analysis of the phylogenetic relationships among the flaviviruses (Family: Flaviviridae) and the evolution of vector transmission. Arch. Virol. **151:**309–325.
14. **Cornish, P. V., S. N. Stammler, and D. P. Giedroc.** 2006. The global structures of a wild-type and poorly functional plant luteoviral mRNA pseudoknot are essentially identical. RNA **12:**1959–1969.
15. **Decker, C. J., and R. Parker.** 1993. A turnover pathway for both stable and unstable mRNAs in yeast: evidence for a requirement for deadenylation. Genes Dev. **7:**1632–1643.
16. **de Vries, A. A., E. D. Chirnside, M. C. Horzinek, and P. J. Rottier.** 1992. Structural proteins of equine arteritis virus. J. Virol. **66:**6294–6303.
17. **Emara, M. M., and M. A. Brinton.** 2007. Interaction of TIA-1/TIAR with West Nile and dengue virus products in infected cells interferes with stress granule formation and processing body assembly. Proc. Natl. Acad. Sci. U. S. A. **104:**9041–9046.
18. **Esteban, R., L. Vega, and T. Fujimura.** 2008. 20S RNA narnavirus defies the antiviral activity of SKI1/XRN1 in Saccharomyces cerevisiae. J. Biol. Chem. **283:**25812–25820.
19. **Eulalio, A., I. Behm-Ansmant, and E. Izaurralde.** 2007. P bodies: at the crossroads of post-transcriptional pathways. Nat. Rev. Mol. Cell. Biol. **8:**9–22.
20. **Fernandez-Garcia, M. D., M. Mazzon, M. Jacobs, and A. Amara.** 2009. Pathogenesis of flavivirus infections: using and abusing the host cell. Cell Host Microbe **5:**318–328.
21. **Garneau, N. L., J. Wilusz, and C. J. Wilusz.** 2007. The highways and byways of mRNA decay. Nat. Rev. Mol. Cell. Biol. **8:**113–126.
22. **Hahn, C. S., Y. S. Hahn, C. M. Rice, E. Lee, L. Dalgarno, E. G. Strauss, and J. H. Strauss.** 1987. Conserved elements in the 3′ untranslated region of flavivirus RNAs and potential cyclization sequences. J. Mol. Biol. **198:**33–41.

23. **Igarashi, A.** 1978. Isolation of a Singh's Aedes albopictus cell clone sensitive to dengue and Chikungunya viruses. J. Gen. Virol. **40:**531–544.
24. **Inoue, H., H. Nojima, and H. Okayama.** 1990. High efficiency transformation of Escherichia coli with plasmids. Gene **96:**23–28.
25. **Jones, C. T., C. G. Patkar, and R. J. Kuhn.** 2005. Construction and applications of yellow fever virus replicons. Virology **331:**247–259.
26. **Kuno, G., G. J. Chang, K. R. Tsuchiya, N. Karabatsos, and C. B. Cropp.** 1998. Phylogeny of the genus Flavivirus. J. Virol. **72:**73–83.
27. **Leathers, V., R. Tanguay, M. Kobayashi, and D. R. Gallie.** 1993. A phylogenetically conserved sequence within viral 3′ untranslated RNA pseudoknots regulates translation. Mol. Cell. Biol. **13:**5331–5347.
28. **Liefhebber, J. M., B. W. Brandt, R. Broer, W. J. Spaan, and H. C. van Leeuwen.** 2009. Hepatitis C virus NS4B carboxy terminal domain is a membrane binding domain. Virol. J. **6:**62.
29. **Lin, K. C., H. L. Chang, and R. Y. Chang.** 2004. Accumulation of a 3′-terminal genome fragment in Japanese encephalitis virus-infected mammalian and mosquito cells. J. Virol. **78:**5133–5138.
30. **Lindenbach, B. D., H. J. Thiel, and C. M. Rice.** 2007. Flaviviridae: the viruses and their replication, p. 1101–1152. *In* D. M. Knipe et al. (ed.), Fields virology, 5th ed. Lippincott Williams & Wilkins, Philadelphia, PA.
31. **Liu, R., L. Yue, X. Li, X. Yu, H. Zhao, Z. Jiang, E. Qin, and C. Qin.** 2010. Identification and characterization of small sub-genomic RNAs in dengue 1–4 virus-infected cell cultures and tissues. Biochem. Biophys. Res. Commun. **391:**1099–1103.
32. **Markoff, L.** 2003. 5′- and 3′-noncoding regions of flavivirus RNA, p. 177–228. *In* T. J. Chambers and T. P. Monath (ed.), The flaviviruses: structure, replication, and evolution. Elsevier Academic Press, Amsterdam, Netherlands.
33. **Matrosovich, M., T. Matrosovich, W. Garten, and H. D. Klenk.** 2006. New low-viscosity overlay medium for viral plaque assays. Virol. J. **3:**63.
34. **Meinkoth, J., and G. Wahl.** 1984. Hybridization of nucleic acids immobilized on solid supports. Anal. Biochem. **138:**267–284.
35. **Men, R., M. Bray, D. Clark, R. M. Chanock, and C. J. Lai.** 1996. Dengue type 4 virus mutants containing deletions in the 3′ noncoding region of the RNA genome: analysis of growth restriction in cell culture and altered viremia pattern and immunogenicity in rhesus monkeys. J. Virol. **70:**3930–3937.
36. **Merino, E. J., K. A. Wilkinson, J. L. Coughlan, and K. M. Weeks.** 2005. RNA structure analysis at single nucleotide resolution by selective 2′-hydroxyl acylation and primer extension (SHAPE). J. Am. Chem. Soc. **127:**4223–4231.
37. **Molenkamp, R., E. A. Kooi, M. A. Lucassen, S. Greve, J. C. Thijssen, W. J. Spaan, and P. J. Bredenbeek.** 2003. Yellow fever virus replicons as an expression system for hepatitis C virus structural proteins. J. Virol. **77:**1644–1648.
38. **Muhlrad, D., C. J. Decker, and R. Parker.** 1994. Deadenylation of the unstable mRNA encoded by the yeast MFA2 gene leads to decapping followed by 5′→3′ digestion of the transcript. Genes Dev. **8:**855–866.
39. **Mutebi, J. P., R. C. Rijnbrand, H. Wang, K. D. Ryman, E. Wang, L. D. Fulop, R. Titball, and A. D. Barrett.** 2004. Genetic relationships and evolution of genotypes of yellow fever virus and other members of the yellow fever virus group within the Flavivirus genus based on the 3′ noncoding region. J. Virol. **78:**9652–9665.
40. **Nixon, P. L., P. V. Cornish, S. V. Suram, and D. P. Giedroc.** 2002. Thermodynamic analysis of conserved loop-stem interactions in P1-P2 frameshifting RNA pseudoknots from plant Luteoviridae. Biochemistry **41:**10665–10674.
41. **Olsthoorn, R. C., and J. F. Bol.** 2001. Sequence comparison and secondary structure analysis of the 3′ noncoding region of flavivirus genomes reveals multiple pseudoknots. RNA **7:**1370–1377.
42. **Parker, R., and U. Sheth.** 2007. P bodies and the control of mRNA translation and degradation. Mol. Cell **25:**635–646.
43. **Pennell, S., E. Manktelow, A. Flatt, G. Kelly, S. J. Smerdon, and I. Brierley.** 2008. The stimulatory RNA of the Visna-Maedi retrovirus ribosomal frameshifting signal is an unusual pseudoknot with an interstem element. RNA **14:**1366–1377.
44. **Pijlman, G. P., A. Funk, N. Kondratieva, J. Leung, S. Torres, L. van der Aa, W. J. Liu, A. C. Palmenberg, P. Y. Shi, R. A. Hall, and A. A. Khromykh.** 2008. A highly structured, nuclease-resistant, noncoding RNA produced by flaviviruses is required for pathogenicity. Cell Host Microbe **4:**579–591.
45. **Plant, E. P., R. Rakauskaite, D. R. Taylor, and J. D. Dinman.** 2010. Achieving a golden mean: mechanisms by which coronaviruses ensure synthesis of the correct stoichiometric ratios of viral proteins. J. Virol. **84:**4330–4340.
46. **Proutski, V., M. W. Gaunt, E. A. Gould, and E. C. Holmes.** 1997. Secondary structure of the 3′-untranslated region of yellow fever virus: implications for virulence, attenuation and vaccine development. J. Gen. Virol. **78:**1543–1549.
47. **Rice, C. M., E. M. Lenches, S. R. Eddy, S. J. Shin, R. L. Sheets, and J. H. Strauss.** 1985. Nucleotide sequence of yellow fever virus: implications for flavivirus gene expression and evolution. Science **229:**726–733.
48. **Sambrook, J., T. Fritsch, and T. Maniatis.** 1989. Molecular cloning: a laboratory manual. Cold Spring Harbor Laboratory Press, Cold Spring Harbor, NY.
49. **Scherbik, S. V., J. M. Paranjape, B. M. Stockman, R. H. Silverman, and M. A. Brinton.** 2006. RNase L plays a role in the antiviral response to West Nile virus. J. Virol. **80:**2987–2999.
50. **Sheth, U., and R. Parker.** 2003. Decapping and decay of messenger RNA occur in cytoplasmic processing bodies. Science **300:**805–808.
51. **Shi, P. Y., M. A. Brinton, J. M. Veal, Y. Y. Zhong, and W. D. Wilson.** 1996. Evidence for the existence of a pseudoknot structure at the 3′ terminus of the flavivirus genomic RNA. Biochemistry **35:**4222–4230.
52. **Silva, P. A., R. Molenkamp, T. J. Dalebout, N. Charlier, J. H. Neyts, W. J. Spaan, and P. J. Bredenbeek.** 2007. Conservation of the pentanucleotide motif at the top of the yellow fever virus 17D 3′ stem-loop structure is not required for replication. J. Gen. Virol. **88:**1738–1747.
53. **Stevens, A.** 1978. An exoribonuclease from Saccharomyces cerevisiae: effect of modifications of 5′ end groups on the hydrolysis of substrates to 5′ mononucleotides. Biochem. Biophys. Res. Commun. **81:**656–661.
54. **Stevens, A.** 1980. Purification and characterization of a Saccharomyces cerevisiae exoribonuclease which yields 5′-mononucleotides by a 5′ leads to 3′ mode of hydrolysis. J. Biol. Chem. **255:**3080–3085.
55. **Su, L., L. Chen, M. Egli, J. M. Berger, and A. Rich.** 1999. Minor groove RNA triplex in the crystal structure of a ribosomal frameshifting viral pseudoknot. Nat. Struct. Biol. **6:**285–292.
56. **Urosevic, N., M. van Maanen, J. P. Mansfield, J. S. Mackenzie, and G. R. Shellam.** 1997. Molecular characterization of virus-specific RNA produced in the brains of flavivirus-susceptible and -resistant mice after challenge with Murray Valley encephalitis virus. J. Gen. Virol. **78:**23–29.
57. **van der Most, R. G., P. J. Bredenbeek, and W. J. Spaan.** 1991. A domain at the 3′ end of the polymerase gene is essential for encapsidation of coronavirus defective interfering RNAs. J. Virol. **65:**3219–3226.
58. **Vreken, P., and H. A. Raue.** 1992. The rate-limiting step in yeast PGK1 mRNA degradation is an endonucleolytic cleavage in the 3′-terminal part of the coding region. Mol. Cell. Biol. **12:**2986–2996.